SIMULATIONS OF MAGNETIC CAPTURING EFFICIENCY OF DRUG CARRIERS IN THE BRAIN VASCULAR SYSTEM

Saša Kenjereš and Bernhard Righolt
Department of Multi-Scale Physics, Faculty of Applied Sciences
and J. M. Burgerscentre for Fluid Dynamics
Delft University of Technology
Leeghwaterstraat 39, 2628 CB Delft
s.kenjeres@tudelft.nl, b.w.righolt@tudelft.nl

ABSTRACT

The present paper reports on numerical simulations of blood flow and magnetic drug carrier distributions in a complex brain vascular system. The blood is represented as a non-Newtonian fluid by generalised power law. The Lagrangian tracking of the multi-layer spherical particles is performed to estimate particle deposition under influence of imposed magnetic field gradients along arterial walls. Two situations are considered: neutral (magnetic field off) and active control (magnetic field on) case. The multi-layer spherical particles that mimic a real medical drug are characterised by two characteristic diameters - the outer one and the inner one of the magnetic core. A numerical mesh of the brain vascular system consisting of multi-branching arteries is generated from raw MRI scan images of a patient. The blood is supplied through four main inlet arteries and the entire vascular system included more than 30 outlets, which are modelled by Murray's law. The no-slip boundary condition is applied for velocity components along the smooth and rigid arterial walls. Numerical simulations revealed detailed insights into blood flow patterns, wall-shear-stress and local particle deposition efficiency along arterial walls. It is demonstrated that magnetically targeted drug delivery significantly increased the particle capturing efficiency in the pre-defined regions. This feature can be potentially useful for localised, non-invasive treatment of brain tumours.

INTRODUCTION

Magnetic Drug Targeting (MDT) is a medical technique based on a relatively simple concept of attaching a therapeutic drug to a small magnetic carrier, which makes it possible to precisely deliver medical drug to the desired location by specifically designed external magnetic field gradients. This localised medical drug delivery enables a significant local increase of the medical drug in regions affected by disease and at the same time reduces the total amount of supplied medical drug. This leads to a significant reduction of the always present negative side-effects of aggressive medical treatments. Experimental studies on animals and pre-clinical studies on human patients demonstrated potentials of this approach as shown in Lübbe et al. (1996a, 1996b) and Alexiou et al. (2006).

Numerical modelling and simulations can provide important insights needed for further advancement and optimisation of the MDT technique - especially in obtaining detailed predictions of local distributions of medical drugs along arterial walls for different sets of the working parameters that include a characteristic particle diameter and different orientations and strengths of an externally imposed magnetic field. In our previous studies we addressed numerical simulations of the MDT technique in simplified and realistic arterial bifurcations (carotid artery, coronary arteries), Kenjereš (2008), Haverkort et al. (2009a, 2009b), Kenjereš and Cohen Stuart (2009). The magnetic drug was simplified to a spherical particle with uniform properties. In the present study, we are extending these simulation to a real-patient brain vascular system. A brain vascular system is a rather complex network of multi-branching arteries. Particular challenge lies in specific anatomic uniqueness of each individual patient that must be included in order to achieve optimised drug delivery. This includes not only the specific geometry of the brain vascular system, but also specific blood flow rates imposed by heartbeats. In addition, a more realistic representation of the multi-layer structure of particles is introduced. It contains a magnetic core and a coated layer of chemotherapeutical drug. The inner magnetic diameter is used in calculating magnetisation force and the outer diameter is used for the drag force.

MATHEMATICAL MODEL

The mathematical model consists of conservative equations for mass and momentum for description of the continuous phase (blood), whereas the discrete phase (particles) is traced in a Lagrangian framework.

Blood flow

The flow of an incompressible non-Newtonian fluid (blood) is described by conservation of momentum:

$$\frac{\partial \rho u_i}{\partial t} + u_j \frac{\partial \rho u_i}{\partial x_j} = -\frac{\partial p}{\partial x_i} + \frac{\partial}{\partial x_j}\left[\mu(\dot{\gamma})\left(\frac{\partial u_i}{\partial x_j} + \frac{\partial u_j}{\partial x_i}\right)\right] \quad (1)$$

and divergency-free velocity field condition ($\partial u_i/\partial x_i = 0$). The blood rheology is taken into account through a generalised power law, Ballyk et al. (1994):

$$\mu(\dot{\gamma}) = \lambda\,|\dot{\gamma}|^{n-1} \quad (2)$$

$$\lambda(\dot{\gamma}) = \mu_\infty + \Delta\mu\; exp\left[-\left(1+\frac{|\dot{\gamma}|}{a}\right)e^{-\frac{b}{|\dot{\gamma}|}}\right] \quad (3)$$

$$n(\dot{\gamma}) = n_\infty - \Delta n\; exp\left[-\left(1+\frac{|\dot{\gamma}|}{c}\right)e^{-\frac{d}{|\dot{\gamma}|}}\right] \quad (4)$$

$$\dot{\gamma} = \sqrt{S_{ij}S_{ji}},\;\; S_{ij} = \frac{1}{2}\left(\frac{\partial u_i}{\partial x_j} + \frac{\partial u_j}{\partial x_i}\right) \quad (5)$$

where $\mu_\infty = 0.0035$ Pa s, $\Delta\mu = 0.025$ Pa s, $n_\infty = 1$, $\Delta n = 0.45$, $a = 50$ s^{-1} , $b = 3$s^{-1}, $c = 50$ s^{-1}, $d = 4$s^{-1}.

Particle motion

The particle tracking is performed using a balance of all active forces

$$m\frac{\partial \vec{v}_p}{\partial t} = \vec{F}_d + \vec{F}_v + \vec{F}_m \quad (6)$$

where $\vec{v}_p$ is the particle velocity, and $\vec{F}_d$, $\vec{F}_v$ and $\vec{F}_m$ are drag, virtual mass and magnetisation force, respectively. The drag force is expressed as:

$$\vec{F}_d = \frac{1}{2}\rho C_D\left(Re_p\right)\left|\vec{u}-\vec{v}_p\right|\left(\vec{u}-\vec{v}_p\right) \quad (7)$$

$$Re_p = \frac{\rho_p D_p\left|\vec{u}-\vec{v}_p\right|}{\mu} \quad (8)$$

where ρ_p and D_p are the particle density and diameter, respectively, and C_D is a coefficient dependent on Re_p, C_D=$24/Re_p$ for $Re_p < 0.1$, and $C_D = 3.69 + 22.73/Re_p + 0.0903/Re_p^2$, for $0.1 \leq Re_p \leq 1$, Morsi and Alexander (1972). The virtual or added mass force is incorporated as

$$\vec{F}_v = \frac{1}{2}\frac{\rho}{\rho_p}\frac{d}{dt}\left(\vec{u}-\vec{v}_p\right). \quad (9)$$

And most importantly, the magnetic force is defined as:

$$\vec{F}_m = V_m \mu_0 \vec{M}\cdot\nabla\vec{H}, \quad (10)$$

with V_m the magnetic core volume, μ_0 the permeability of free space, $\vec{M}$ the magnetisation force per unit area, and $\vec{H}$ the auxiliary magnetic field. In the present model, the particles are assumed to be fully saturated by the magnetic field, which reduces to $\vec{M} = M_{sat}\vec{H}$, with M_{sat} the saturation magnetisation, which is a material property. Furthermore, the gravitational force on the particle is neglected, since it has a $\mathscr{O}\left(10^{-3}\right)$ contribution compared to the magnetisation force. Since a very diluted concentration of the injected medical drug is imposed, we assumed one-way coupling between particles dynamics and blood flow.

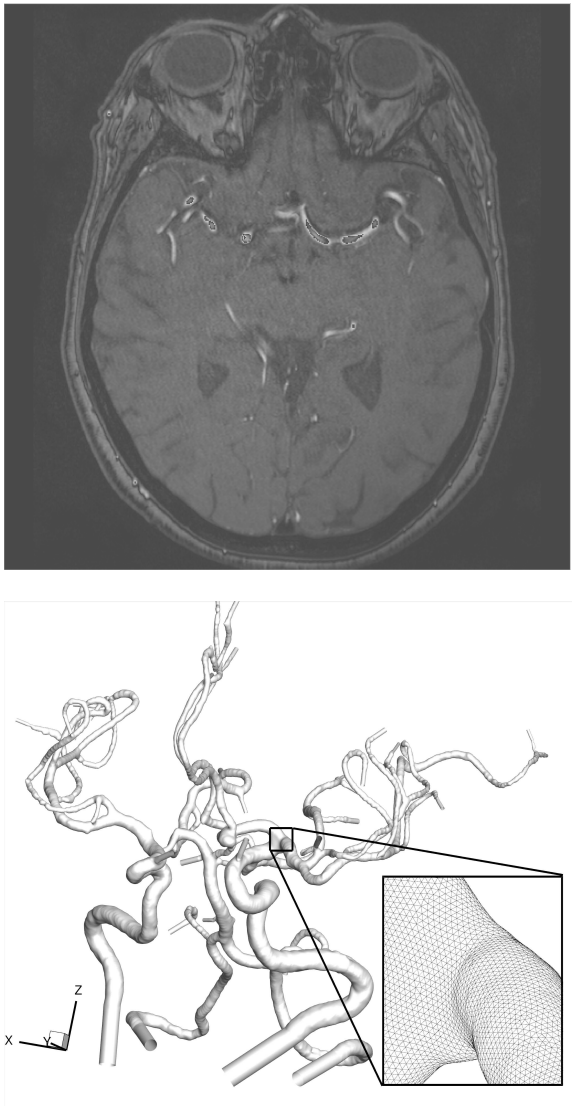

Figure 1: Top- Example of a raw MRI image with an enhanced contrast agent in the brain vascular system. White contrast indicates brain blood vessels in the particular horizontal slice. Bottom- reconstructed 3D geometry and a detail of the tetrahedral numerical mesh in one of the bifurcation regions.

Particle capture

The wall-particle interactions are assumed to be fully inelastic, i.e. a particle that reaches the artery wall will remain there. To provide more precise estimations of the particle deposition efficiency, two quantities were analysed. The radial

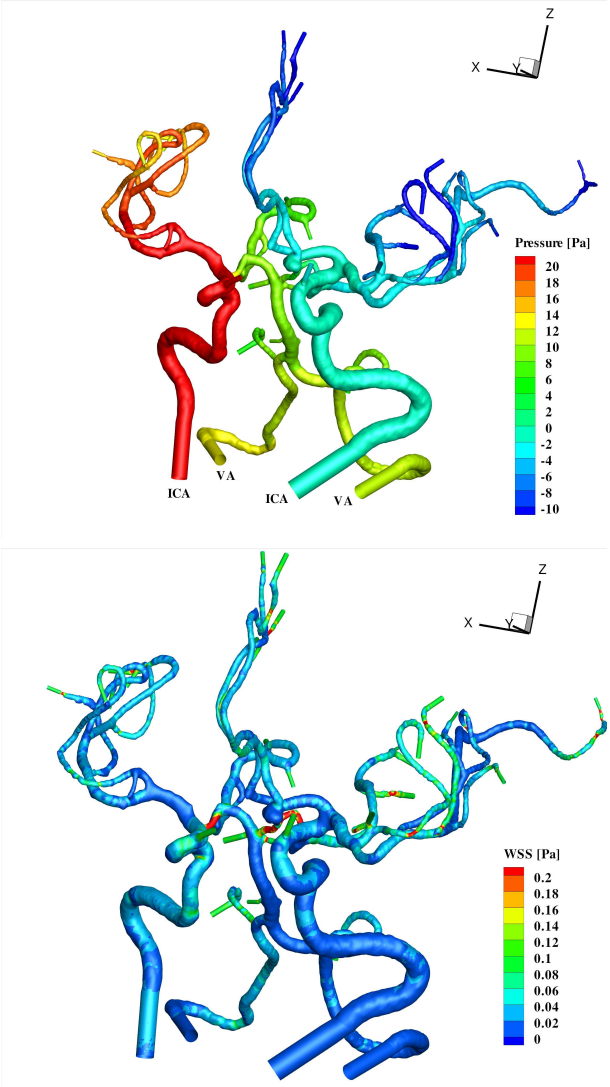

Figure 2: Contours of the pressure (-top) and wall-shear-stress (WSS) (-bottom) distributions along the arterial wall. All inlets are located at the bottom side of the domain and labelled with either ICA (internal carotid artery) or VA (vertebral artery).

capture efficiency represents the relative amount of particles deposited along the arterial walls within a sphere of radius r from the targeted location (e.g. tumour location, $\vec{x}_{tumour}$), and is calculated as

$$\eta(r) = \frac{n_{wall}\left(\left|\vec{x}_{p,i} - \vec{x}_{tumour}\right| < r\right)}{n_{in}}. \tag{11}$$

where n_{wall} is the number of particles deposited along the arterial walls, n_{in} is the total number of injected particles and $\vec{x}_{p,i}$ is the deposition location of i-th particle. This parameter can be interpreted as a cumulative particle deposition efficiency. We also introduced an estimate of the local capturing efficiency, which describes the relative amount of particles deposited along the arterial wall within a pre-specified neighbourhood $N(\vec{x}, \varepsilon)$ as

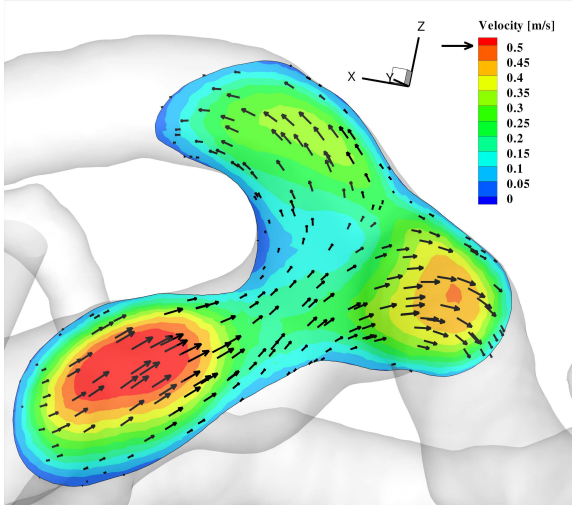

Figure 3: Contours of the velocity magnitude and velocity vector projections in characteristic bifurcation plane.

$$\zeta(\vec{x}) = \frac{n_{wall}\left(\left|\vec{x}_{p,i} - \vec{x}\right| < \varepsilon\right)}{n_{in}}. \tag{12}$$

where ε is the characteristic sample distance. This parameter can be interpreted as a local particle deposition efficiency.

NUMERICAL METHOD

The fluid flow and particle motion equations are discretised and solved by a second-order accurate finite-volume numerical solver for unstructured geometries. The time integration is performed by a fully-implicit three-consecutive time-step method. The diffusive and convective terms are discretised by a second-order upwind difference scheme.

Employing a similar approach to that of Antiga et al. (2008) and Nunduri et al. (2009), a numerical mesh of the brain vascular system consisting of multi-branching arteries is generated from raw MRI scan images of a real patient, Fig. 1. Initial transient simulations (pulsating blood cycles) are performed for a reduced brain vascular geometry that includes only one main inlet artery (carotid artery) and about ten outlets. It is concluded that a time-dependency of flow does not significantly affect particle deposition along the arterial walls, and we focused our investigations to a more detailed geometrical model of the brain vascular system with steady inflow conditions. The flow rates through internal carotid (275 ml/min) and vertebral (91 ml/min) arteries are specified in accordance to measurements presented in Ford et al. (2005). The maximum Reynolds number based on characteristic diameter of the largest carotid artery is 460 indicating that blood flow is in a laminar regime. The outflow rates are modelled by Murray's law in order to compensate down-flow resistance of smaller brain arteries as

$$\sum_i R_{in,i}^3 = \sum_j R_{out,j}^3 \;\; or \;\; \sum_i \phi_{v,in,i} = \sum_j \phi_{v,out,j}, \tag{13}$$

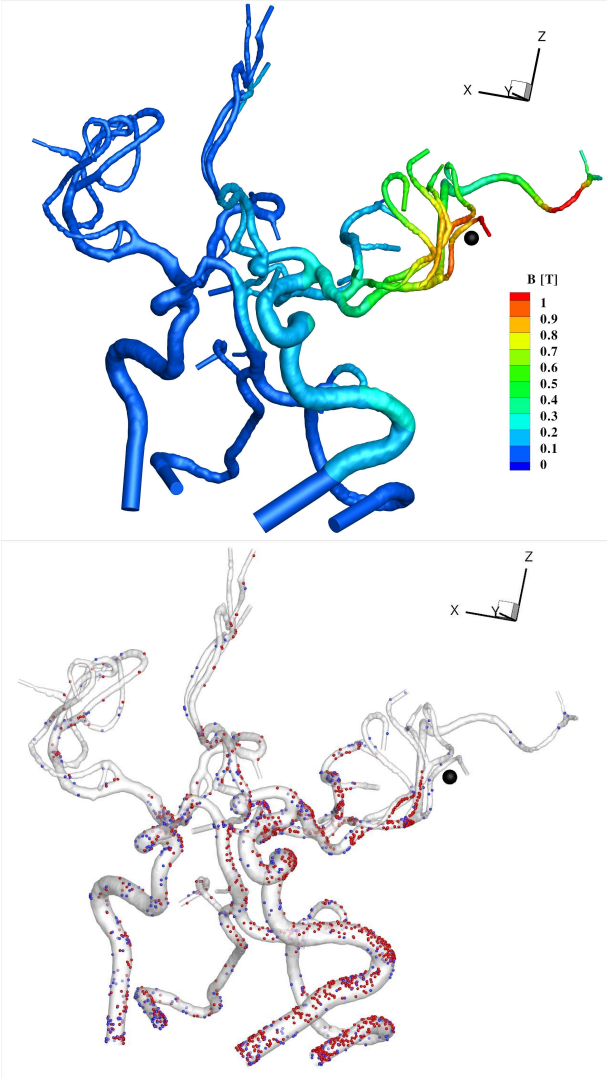

Figure 4: The magnetic field strength is shown along the arterial walls. The black sphere on the right indicates the assumed location of a tumour (-top). Particles captured (red-with magnetic field, blue-without magnetic field) at their respective locations, for $D_p = 0.5\mu$ m, V_p/V_m=1 (-red), V_p/V_m=∞ (-blue) class of particles (-bottom).

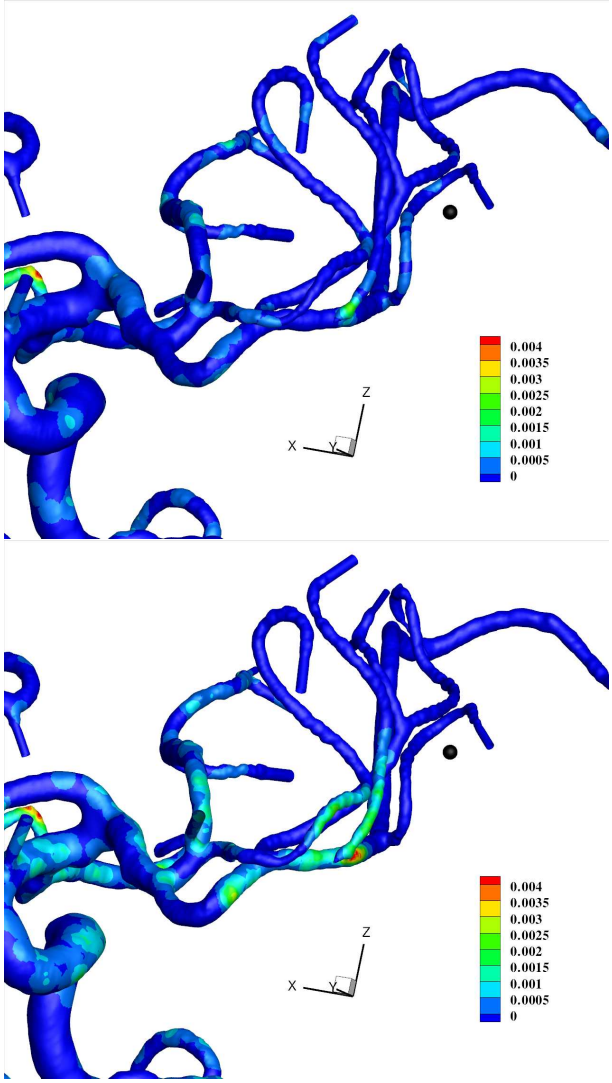

Figure 5: A zoom-in of the particle ($D_p = 0.5\mu$m) deposition efficiency (ζ) along the arterial walls - without (V_p/V_m=∞) (-top) and with (V_p/V_m=1) (-bottom) imposed magnetic field.

with $R_{in,i}$ the radius of the i-th inflow (i=1 to 4 in our case), $R_{out,j}$ the radius of the j-th outflow (j=1 to 31 in our case) and the ϕ_v is characteristic flow rate, Olufsen (1999). The entire brain vascular system geometry is represented by approximately 5.1×10^6 tetrahedral control volumes, which were sufficient to obtain grid-independent results. The brain vascular geometry is constructed from raw MRI images shown in Fig. 1. Particles are injected homogeneously over four inlets and their trajectories are traced by a fourth-order Runge-Kutta scheme. Different classes of particles are considered, ranging from 0.25 μm to 4 μm. The particle density is ρ_p=6450 kg/m^3 with a saturation magnetisation of M_{sat}=10^6 A/m. Density of the coated layer is ρ_c=1610 kg/m^3, that closely corresponds to the chemotherapeutical drug Epirubicin. The blood density is ρ=1050 kg/m^3. For each class of particles, different ratios of the outer and magnetic core volumes $\frac{V_p}{V_m} \in \{1,2,4,8,\infty\}$ are analysed. Here V_p/V_m=1 corresponds to pure magnetic carrier, and V_p/V_m=∞ to a pure medical drug particle (without magnetic core), respectively. Characteristic values of Stokes numbers based on characteristic particle and arterial diameters are in $1.9\times10^{-7} \leq St \leq 2.3\times10^{-4}$ range.

RESULTS

Flow details

Contours of the pressure and the wall-shear-stress (WSS) along the arterial walls are shown in Fig. 2. The four main inlets are marked with ICA (internal carotid artery) and VA (vertebral artery). Note the asymmetrical distribution of the pressure field due to anatomical differences between the left and right side of the brain vascular system. It can be seen that the local maxima of the WSS (defined as $\tau_W = \mu(\dot{\gamma})\partial v_{\|}/\partial n$)

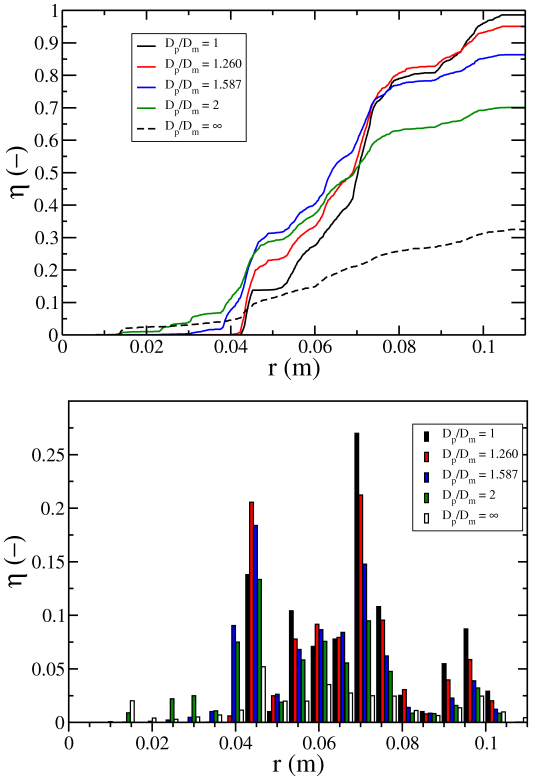

Figure 6: Cumulative (-top) and histograms of the local (-bottom) radial capturing efficiency along arterial walls for $D_p = 2\mu$m class of particles.

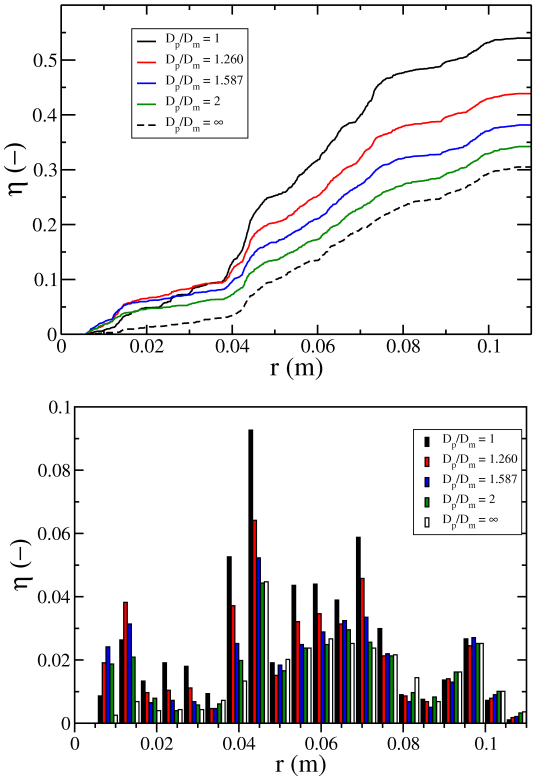

Figure 7: Same as in the previous Figure, only for $D_p = 0.5\mu$m particles.

are located at arterial bifurcations. Projections of the velocity vectors and contours of the velocity magnitude in a characteristic bifurcation are shown in Fig. 3.

Magnetic field

In order to mimic targeted drug delivery, an externally imposed superconductive magnet is introduced, Haverkort et al. (2009b). The origin, orientation and strength of the imposed magnetic field can be easily manipulated in order to cover the desired location. For example, in order to target a small brain tumour (dark circle), the origin of the magnetic field source is located at a distance of 3 cm away from the head, and its spatial distribution is shown in Fig. 4-top. Locations of captured particles (red- for magnetic field on, blue-magnetic field off) along arterial walls are shown in Fig. 4-bottom. It can be seen that the red particles are more concentrated in the right side of the brain vascular system, confirming enhanced deposition due to imposed magnetic field.

Particle location

To introduce a more objective quantification of the particle capturing, contours of the local particle deposition efficiency (ζ, with ε=1 mm, Eq. 12) are shown in Fig. 5. The zoom-ins indicate that in contrast to a neutral case (Fig. 5-top) where only arterial bifurcations generate a local increase of deposited particles, for the magnetically active case (Fig. 5-bottom), also arteries in the proximity of the tumour show significantly increased levels of deposited particles. Now we will focus on more detailed analysis of different classes of particles and with different ratios of particle/magnetic core diameters, i.e. of different thickness of the coated layer of a medical drug around a magnetic core. For D_p/D_m=∞, it simply means that there is no magnetic core present, i.e. particles do not feel the presence of the imposed magnetic field gradient. First conclusion from Figs. 6-8 is that bigger particles show more effective capturing by imposed magnetisation force, what is expected, since this force scales as $\vec{F}_m \propto d_m^3$. Here the upper limit for the particle diameter is determined by characteristic size of the micro-capillary vessels (D_p<4μm). The cumulative capturing efficiency for D_p=2μm reaches almost 100% for D_p/D_m=1, Fig. 6-top. Of course, for medical treatments, it is always necessary to have $D_p/D_m > 1$ in order to be able to deliver some amount of the medical drug attached to the magnetic carrier. By doubling this ratio, i.e. for D_p/D_m=2, the total capturing efficiency η=0.7, which is twice as efficient as the neutral case (systemic delivery without magnetic field). The increased capturing efficiency is also observed for D_p=0.5μm and D_p=0.25μm class of particles, Figs. 7 and 8-top, but now η reaches maximum values of 0.55 and 0.375, respectively. Note that for the biggest class of particles D_p=2μm, in the region very close to the tumour location ($r \leq 0.04$ m), deposition efficiency is very small. This is a consequence of the more efficient capturing in more distant regions - making practically all particles captured before reaching the desired location. The histograms (with characteristic bin length of 5.5 mm) of the local deposition efficiency

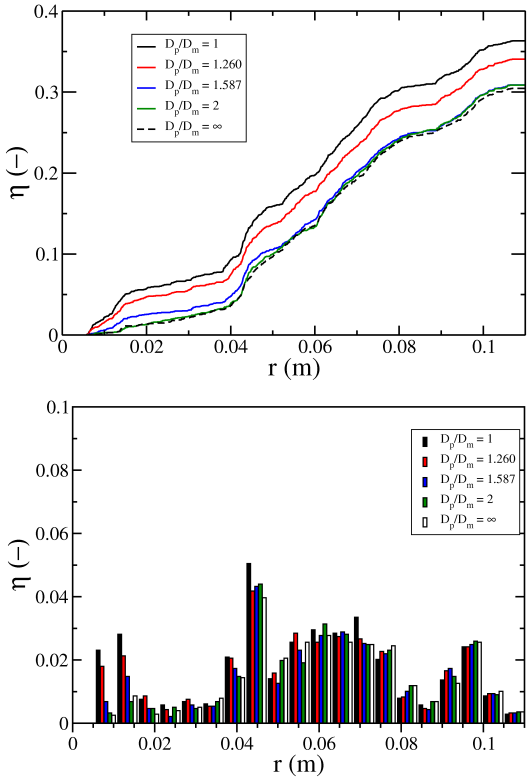

Figure 8: Same as in the previous Figure, only for $D_p = 0.25\mu$m particles.

(ζ) show more than tenfold increase in localised capturing efficiency for $D_p = 2\mu$m class of particles in $0.06 \leq r \leq 0.08$ segment when magnetic targeting is activated, Fig. 6-bottom. For D_p=0.5μm class of particles, a maximum of fivefold increase is observed in the proximity of $r = 0.05$ m location. For the smallest class of particles, D_p=0.25μm, this increase is just marginal, indicating lower limits of particles diameter in order to make magnetic drug delivery efficient.

CONCLUSION

The one-way coupled simulations of the non-Newtonian fluid (blood) flow and multi-layered particles with a magnetic core are performed for a complex, patient based, multi-branching brain vascular system. The numerical mesh is efficiently constructed from slices of the raw MRI scans. It is demonstrated that application of the magnetic drug delivery technique leads to a significant increase of the captured medical drug in targeted regions. The wide range of the particle diameters and relative volumes of the magnetic cores is analysed in detail. It is found that for a given imposed magnetic field, efficiency of the magnetic capturing depends on underlying blood flow patterns (bifurcations, three-dimensionality of flow, sudden acceleration or de-acceleration of flow due to specific anatomic details) and size of the injected particles. Numerical simulations proved to be a powerful tool for further development of the MDT technique for patient-specific clinical studies.

Acknowledgement

Dr. Patrick Brouwer and Jasper Janssen MSc. from Radiology and Neurosurgery Department, Leiden University Medical Centre, Leiden, The Netherlands are gratefully acknowledged for providing a specific patient MRI scan. Mr. Alex de Mulder is acknowledged for his assistance in mesh generation from the raw MRI scans.

REFERENCES

C. Alexiou, R. J. Schmid, R. Jurgons, M. Kremer, G.Wanner, C. Bergemann, E. Huenges, T. Nawroth, W. Arnold, and F. G. Parak, 2006, "Targeting cancer cells: magnetic nanoparticles as drug carriers", Eur. Biophysics J., Vol. 35, pp. 446–450.

L. Antiga, M. Piccinelli, L. Botti, B. Ene-Iordache, A. Remuzzi and D. A. Steinman, 2008, "An image-based modelling framework for patient-specific computational hemodynamics", Med. Biol. Eng. Comp., Vol.46, pp. 1097–1112.

P. D. Ballyk, D. A. Steinman and C. R. Ethier, 1994, "Simulation of non-Newtonian blood flow in an end-to-side anastomosis", Biorheology, Vol.31 (5), pp. 565–586.

J. W. Haverkort, S. Kenjereš and C. R. Kleijn, 2009a, "Magnetic particle motion in a Poiseuille flow", Phys. Rev. E **80** (1), Art. No. 016302, pp. 1–12.

J. W. Haverkort, S. Kenjereš and C. R. Kleijn, 2009b, "Computational Simulations of Magnetic Particle Capture in Arterial Flows", Annals of Biomedical Engineering **37** (12), pp. 2436–2448.

S. Kenjereš, 2008, "Numerical analysis of blood flow in realistic arteries subjected to strong non-uniform magnetic fields", Int. J. Heat and Fluid Flow, Vol.29 (3), pp. 752–764.

S. Kenjereš and D. C. Cohen Stuart, 2009, "Computational simulations of magnetic particle capture in simplified and realistic arterial flows: towards optimized magnetic drug targeting", Proceedings of World Congress on Medical Physics and Biomedical Engineering, 7-12 September 2009, Munich, Germany, IFMBE Proceedings, Vol.25 (4), pp. 1006–1009.

A. S. Lübbe, C. Bergemann, H. Riess, F. Schriever, P. Reichardt et al., 1996a, "Clinical experiences with magnetic drug targeting: A phase i study with 4'-epidoxorubicin in 14 patients with advanced solid tumors", Cancer Research, Vol.56 (20), pp. 4686-4693.

A. S. Lübbe, C. Bergemann, W. Huhnt, T. Fricke, H. Riess, J. W. Brock and D. Huhn, 1996b, "Preclinical Experiences with Magnetic Drug Targeting: Tolerance and Efficacy", Cancer Research, Vol.56 (20), pp. 4694–4701.

S. A. Morsi and A. J. Alexander, 1972, "An investigation of particle trajectories in two-phase flow systems", J. Fluid Mech., Vol.55 (2), pp. 193–208.

J. R. Nanduri, F. A. Pino-Romainville and I. Celik, 2009, "CFD mesh generation for biological flows: Geometry reconstruction using diagnostic images", Computers and Fluids, Vol.38, pp. 1026–1032.

M. S. Olufsen, 1999, "Structured tree outflow condition for blood flow in larger systemic arteries", Am. J. Physiol. Heart Circ. Physiol., Vol.276, pp. 257–268.